Applied Composite Materials (2025) 32:149–172
https://doi.org/10.1007/s10443-024-10268-3

RESEARCH

Efficient Approximation of Varying Fiber Orientation States in Injection Molded Parts Under Consideration of Multiple Manufacturing Uncertainties

Florian Wittemann[1] · **Constantin Krauß**[1] · **Luise Kärger**[1]

Received: 31 May 2024 / Accepted: 30 August 2024 / Published online: 2 October 2024

Abstract
The production of high-quality fiber reinforced polymer parts is an important aspect in several industrial areas. However, due to unavoidable uncertainties in material and manufacturing processes, the part quality scatters. One important aspect here is the fiber orientation, being crucial for the thermo-mechanical properties of the part and being influenced by the uncertain material state and process conditions. Process simulations are an important tool for predicting the fiber orientation, but state-of-the-art simulations are normally deterministic and represent only one specific case. Performing enough deterministic simulations to model manufacturing uncertainties requires high numerical effort. Therefore, this work presents methods to quickly and efficiently approximate the fiber orientation under varying material and process parameters, requiring only a few simulations as input. Different schemes for approximation are evaluated and compared with each other and with 3D process simulations.

Keywords Discontinuous fiber reinforced polymers · Injection molding simulation · Process uncertainties · Fiber orientation approximation

1 Introduction

Discontinuous fiber reinforced polymers (FRPs) are becoming more important for structural and semi-structural parts. The materials are compounded to a fiber-matrix-suspension, where the fibers are more or less able to move and orientate within the matrix. Therefore, discontinuous FRPs are well suited for mold filling processes and complex geometrical features. During the manufacturing of FRP parts, the fibers re-orientate and the final orientation has crucial impact on the final part's thermo-mechanical properties. Especially in processes with long flow paths like injection or compression molding, the process conditions influence the flow field and therefore the fiber orientation. Thus, the manufacturing itself has an impact on the final part's properties.

✉ Florian Wittemann
florian.wittemann@kit.edu

[1] Present Address: Institute of Vehicle System Technology, Lightweight Engineering Division, Karlsruhe Institute of Technology (KIT), Rintheimer Querallee 2, Karlsruhe 76131, Germany

To predict the final fiber orientation, process simulation is an important tool. Such process simulations are normally non-isothermal and transient computational fluid dynamics (CFD) simulations, which are numerically solved on finite elements [1] or finite volumes [2–7]. Due to the numerical effort, the fiber matrix suspension is described with a homogenized material modeling approach and the orientation state is given by orientation tensors [8]. The orientation evolution is dominated by the flow field, where the material's viscosity is the most important property for flow modeling. According to the state of the art, polymer viscosities are modeled temperature and shear rate dependent, where for thermoplastics the so-called Cross-WLF approach is most common [9]. In case of thermoset materials, additionally the curing reaction is relevant and the most common viscosity approach is the Castro-Macosko model [10]. Most state-of-the-art simulation tools model the viscosity isotropic, even though the fibers influence the flow field in an anisotropic way. More advanced approaches consider fiber aspects in the viscosity modeling to gain a coupled flow and fiber orientation modeling [4, 7, 11].

Nevertheless, all these approaches describe mold filling and fiber orientation deterministically for a specific combination of given material properties and boundary conditions. In reality, process and material underly natural and environmentally triggered uncertainties, leading to scatter in part production and eventually to uncertainties of the final fiber orientation and part properties. Process conditions, for example material temperature, influence the part properties, as presented by Jansen et al. [12] and Kurt et al. [13], who investigated the influence on shrinkage in thermoplastic injection molding. Mesogitis et al. [14] name material conditions like storage, pre-curing, contaminations, humidity, etc. as important aspects for process and part property uncertainties for mold filling with thermoset matrix materials. These uncertainties lead to raising safety factors, which cause inefficient material use, with negative impact on the lightweight potential and ecological footprint of the produced parts. To quantify the consequences of material and process uncertainties on part properties, knowledge about the uncertainty of fiber orientation is one indispensable information. The uncertainty of the orientation can be predicted by simulations. However, since today's modeling approaches for mold filling simulations with FRPs are deterministic, a prediction of uncertainty would only be possible by performing several process simulations with varying input parameters for material attributes (e.g. initial curing state and fiber length) and process conditions (e.g. temperature of tool and material). Performing such a high number of process simulations with varying combinations of uncertain input parameters means high computational effort, which is not capable at the moment within a meaningful period of time. One solution to overcome this problem is an efficient approximation of the resulting fiber orientations for a given combination of input parameters, based on just a single detailed and time-consuming process simulation. This work presents such an approximation scheme for injection molded FRPs with arbitrary combinations of uncertain input parameters regarding material temperature, tool temperature, initial curing state and fiber length.

Starting point is a parameter variation of material and tool temperature, fiber length and initial curing state for thermoset injection molding to quantify the influence of these parameters on the final fiber orientation. The data is then used to develop interpolation-based schemes, which approximate the fiber orientation due to multiple parameter variations in a wide range. For that purpose, the orientations tensors need to be interpolated. In contrast to scalar fields, e.g., temperature, pressure, etc., the interpolation of tensor-valued fields is significantly less studied and understood in engineering contexts. Naive adaption of scalar techniques to tensorial data is widely applied but found to induce artificial bias towards isotropic states [15, 16]. As alternative approach, several contributions propose decomposition-based

techniques, which interpolate direction-dependent and direction-independent characteristics separately [17, 18]. Very recently, those techniques have been generalized to accept fiber orientation tensors as input confirming the superiority of decomposition-based techniques for relevant experimental and numerical use-cases [19, 20]. It should be noted however, that all of these approaches are applied for spatial interpolation, i.e. the interpolation functions take three-dimensional coordinates as input. In the present study, however, interpolation is intended to operate on a multi-dimensional parameter space, where possible (auto-)correlation of arguments must be considered.

Therefore, four different approaches are compared and the scheme creating the best results is used to efficiently create orientation data with random input parameters. The approximations are in good agreement with full 3D-simulation.

2 Process Simulation for Uncertainty Quantification

2.1 Simulation Approach

The process simulations within this work are performed with the open-source FVM-solver package OpenFOAM®. A detailed description of the Methodology, Material models and implementation is given in [3, 4, 21]. The most relevant aspects of the process simulations for this work, being fiber orientation modeling and viscosity modeling, are described in more detail in Sect. 2.1.1 and 2.1.2. Since thermoset injection molding is in focus of this study, curing kinetics are involved and modeled with the Kamal-Malkin approach [22]. The fiber orientation evolution is determined by a second-order orientation tensor, according to the work of Advani and Tucker [8]. The RSC model, presented by Wang et al. [23], is used for fiber orientation evolution. The IBOF5 approach [24] is used for closure approximation. This combination of modeling approaches was validated by the authors in [4, 6] and proved to be suitable to simulate the injection molding process with discontinuous short fiber reinforced thermoset materials.

2.1.1 Fiber Orientation Model

Today's fiber orientation models are nearly all based on the work of Jeffery [25], describing the motion of a single ellipsoidal particle surrounded by an infinite Newtonian fluid. Due to its formulation, Jeffery's approach does not allow steady-state orientation states, but this phenomenon is typical for non-dilute fiber-reinforced polymers with a sufficiently large flow path. Therefore, Folgar and Tucker [26] presented one of the first approaches to model fiber orientation in FRPs by expanding Jeffery's approach with an additional term, containing the so-called interaction coefficient C_I, which allows for diffusion towards steady-state orientation states. Since it is numerically not capable to model the motion of every single fiber, the evolution of fiber orientation is often represented by orientation tensors according to Advani and Tucker [8].

Fiber orientation modeling in this work is performed with the reduced strain closure (RSC) model by Wang et al. [23], representing the orientation evolution by

$$\frac{d\boldsymbol{A}}{dt} + \boldsymbol{U}\frac{\partial \boldsymbol{A}}{\partial \boldsymbol{x}} = (\boldsymbol{W}\boldsymbol{A} - \boldsymbol{A}\boldsymbol{W}) + \frac{r_\mathrm{f}^2 - 1}{r_\mathrm{f}^2 + 1}\{\boldsymbol{D}\boldsymbol{A} + \boldsymbol{A}\boldsymbol{D} - 2[\mathbb{A} + (1-\kappa)(\mathbb{L} - \mathbb{M}\mathbb{A})]\boldsymbol{D}\} + 2\kappa C_\mathrm{I}\dot{\gamma}(\boldsymbol{I} - 3\boldsymbol{A}), \tag{1}$$

where $\boldsymbol{A}$ and $\mathbb{A}$ are the second- and fourth-order orientation tensor according to Advani and Tucker [8], $\boldsymbol{U}$ is the velocity, $\boldsymbol{x}$ is the coordinate vector and t represents the time. $\boldsymbol{W}$ and $\boldsymbol{D}$ are the vorticity and strain rate tensor, $\dot{\gamma}$ the scalar shear rate and r_f the fibers' aspect ratio. $\boldsymbol{I}$ represents the second-order identity tensor, and $\mathbb{L}$ and $\mathbb{M}$ are calculated with the eigenvalues and eigenvectors of $\boldsymbol{A}$ [23]. The strain reduction factor $\kappa \in [0,1]$ represents the main difference between the RSC and Folgar-Tucker approach, since the two approaches are identical for $\kappa = 1$. In general, the orientation evolution, meaning the rotation of fibers and therefore alignment in flow direction, is slower for smaller values of κ.

For any considered fiber length within this work, it is $\Phi_\mathrm{f} r_\mathrm{f} > 1$, with Φ_f being the fiber volume fraction. So according to Advani [27], the interaction coefficient C_I is calculated as presented by Bay [28] that

$$C_\mathrm{I} = 0.0184 \exp\left(-0.7148 \Phi_\mathrm{f} r_\mathrm{f}\right). \tag{2}$$

Hence, a variation of fiber length directly influences the fiber orientation modeling by changing the fiber aspect ratio and therefore the term $(r_\mathrm{f}^2 - 1)/(r_\mathrm{f}^2 + 1)$ in the orientation model and the calculation of C_I.

2.1.2 Viscosity Model

The simulation approach for the viscosity of the FRP presented in [4] represents the material viscosity with a fourth-order viscosity tensor

$$\begin{aligned} \boldsymbol{\eta}_{\mathbf{IV}} = &\left(\eta_{11} - 4\eta_{12} + \eta_{23}\right)\mathbb{A} \\ &+\left(-\tfrac{\eta_{11}}{3} + \eta_{23}\right)(\boldsymbol{A} \otimes \boldsymbol{I} + \boldsymbol{I} \otimes \boldsymbol{A}) \\ &+\left(\eta_{12} - \eta_{23}\right)\left(\boldsymbol{A}\square\boldsymbol{I} + (\boldsymbol{A}\square\boldsymbol{I})^{\mathrm{T_R}} + \boldsymbol{I}\square\boldsymbol{A} + (\boldsymbol{I}\square\boldsymbol{A})^{\mathrm{T_R}}\right) \\ &+\left(\tfrac{\eta_{11}}{9} - \eta_{23}\right)(\boldsymbol{I} \otimes \boldsymbol{I}) \\ &+\eta_{23}\left(\boldsymbol{I}\square\boldsymbol{I} + (\boldsymbol{I}\square\boldsymbol{I})^{\mathrm{T_R}}\right), \end{aligned} \tag{3}$$

with

$$\begin{aligned} \eta_{11} &= \tfrac{\eta_\mathrm{M}\Phi_\mathrm{f}}{2}\left(\tfrac{\sqrt{\Phi_\mathrm{f}/\Phi_\mathrm{max}}}{1-\sqrt{\Phi_\mathrm{f}/\Phi_\mathrm{max}}}\right) r_\mathrm{f}^2, \\ \eta_{12} &= \tfrac{\eta_\mathrm{M}}{2}\left(\tfrac{2-\sqrt{\Phi_\mathrm{f}/\Phi_\mathrm{max}}}{1-\sqrt{\Phi_\mathrm{f}/\Phi_\mathrm{max}}}\right), \\ \eta_{23} &= \tfrac{\eta_\mathrm{M}}{\left(1-\Phi_\mathrm{f}/\Phi_\mathrm{max}\right)^2}, \end{aligned} \tag{4}$$

considering matrix viscosity η_M, fiber length (via aspect ratio r_f) as well as the fiber orientation state by $\boldsymbol{A}$ and $\mathbb{A}$. Φ_max is the maximum possible fiber volume fraction, assumed to be $\pi/\sqrt{12}$ (hexagonal packing) [29]. Therefore, fiber re-orientation and fiber length variations are captured in the flow modeling, which is important for modeling process uncertainties. The definitions of η_{11}, η_{12} and η_{23} are according to Pipes et al. [29]. To calculate the matrix viscosity η_M, the approach by Castro and Macosko [10] is used with

$$\begin{aligned} \eta_\mathrm{M} &= \frac{\eta_0}{1+\left(\frac{\eta_0\dot{\gamma}}{\tau^*}\right)^{1-n_\mathrm{CM}}}\left(\frac{c_\mathrm{g}}{c_\mathrm{g}-c}\right)^{(c_1+c_2 c)}, \\ \eta_0 &= B_\mathrm{CM}\exp\left(\frac{T_\mathrm{B}}{T}\right), \end{aligned} \tag{5}$$

where $n_{CM}, \tau^*, B_{CM}, T_B, c_1$ and c_2 are material specific constants, T the temperature, c the degree of cure and c_g the gelation point. Hence, the process and material uncertainties of varying material and tool temperatures as well as varying initial curing states are captured in the flow modeling.

2.1.3 Simulation Model and Material

According to experimental tests performed in [30] the simulated material is a 22.3 vol.-% glass fiber filled phenolic. Based on measurements, the fibers are assumed to have an average length of 0.38 mm and a constant diameter of 0.017 mm. Due to the short fiber length, it is assumed that the fiber length stays constant and therefore no fiber breakage is considered in the simulations within this work. In consultation with the material supplier, the initial curing state is assumed to be 10%. The material is injected with a temperature of 120 °C and the mold is heated to 175 °C. The mold is filled with a constant volume flow of 75 cm^3/s. This configuration will be called 'reference case' in the following.

The simulated cavity is a rectangular plate with 480 mm × 190 mm × 2 mm as shown in Fig. 1. The material enters the plate via a 185 mm long cone sprue at the plate's center, having a start diameter of 9 mm and an end diameter of 15.5 mm. For the simulation, the cavity is meshed with hexahedral elements. In the plate, the cell size is 2.3 mm in x_1-, 1.75 mm in x_2- and 0.25 mm in x_3-direction. The nozzle and sprue are discretized with 32 cells along the circumference, 24 along the diameter and 140 in x_3-direction. For the screw chamber, 64 cells along the circumference and 72 cells in radial direction are used, with a x_3-dimension of the cells of 1.57 mm.

The fiber orientation will be evaluated at eleven points with different x_1- and x_2-coordinates (P_1 to P_{11}) illustrated in Fig. 2. Due to the symmetry of the plate, these eleven points represent the complete plate. Since the simulation is performed using eight finite volume cells over plate thickness, also eight orientation tensors over plate thickness exist at P_1 to P_{11} (represented by the cell centers). Consequently, 88 points within the simulation model are considered and the multi-dimensional parameter-space interpolation is performed at these 88 points. As mentioned, no spatial interpolation of tensors is needed within this work. Therefore, the shown approaches are only applicable if all input data and the output data refer to identical meshes.

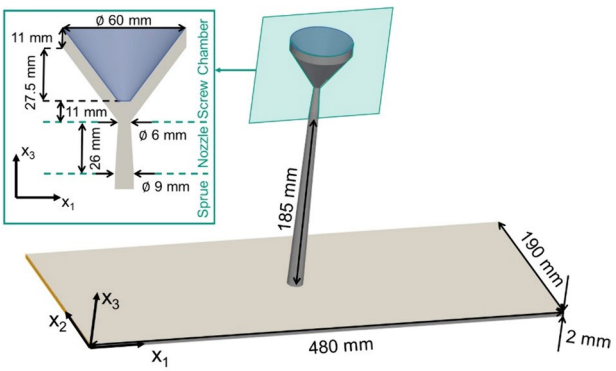

Fig. 1 Geometry for injection molding simulation. Inlet area in blue and outlet in orange

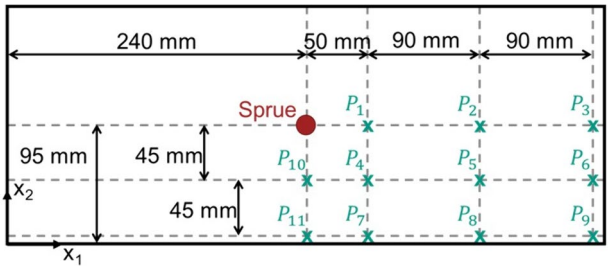

Fig. 2 Top view on the simulated plate. Positions P_1 to P_{11} for evaluation and comparison of fiber orientations resulting from 3D process simulations and from parameter-space interpolation

2.2 Parameter Variations and Process Simulation Results

2.2.1 Parameter Variations

The varied parameters are tool temperature T_{Tool}, initial material temperature T_{Mat}, fiber length L_{F} and initial degree of cure c_0. The reference values and variation steps are given in Table 1. The parameters T_{Tool} and T_{Mat} are varied only to a maximum of $\pm 10\%$, since these are process parameters, with a lower uncertainty compared to material parameters. The temperature variation is based on °C scale, so T_{Mat} $+10\%$ corresponds to 132 °C.

In a first step, 45 full 3D process simulations are performed with the methods described in Sect. 2.1. One simulation is the reference case with the nominal values of the real process, given in Table 1. The other 44 simulations are single realizations of one parameter variation according to Table 1. The intervals of input parameter variation are chosen on experience, not on actual measured values, since the focus of this work is the general feasibility of a multi-dimensional parameter-space interpolation of orientation tensors, not the actual quantification of individual parameter uncertainties.

2.2.2 Fiber Orientation Results for Parameter Variation

In this section, the influence of the four varied parameters T_{Tool}, T_{Mat}, L_{F} and c_0 on the simulated fiber orientation is evaluated. The parameter variation is given in Table 1. The results are shown in Fig. 3 for P_1, Fig. 4 for P_2 and Fig. 5 for P_3 (cf. Fig. 2). The reference simulation is given in green, variations with negative percent deviations in blue and positive percent deviations in red.

In general, lowering T_{Tool} leads to higher viscosities and therefore raises the simulated value of A_{11}. In contrast, rising T_{Mat} or c_0 also rises the predicted value of A_{11} by rising the viscosity due to a higher degree of cure. It would have been expected that a

Table 1 Varied parameters with corresponding reference values and variation steps

Parameter	Reference value	Variation in % ±2.5	±5	±7.5	±10	±15	±25	±50
T_{Tool}	175 °C	✓	✓	✓	✓	✗	✗	✗
T_{Mat}	120 °C	✓	✓	✓	✓	✗	✗	✗
L_{F}	0.38 mm	✓	✓	✓	✓	✓	✓	✓
c_0	10 %	✓	✓	✓	✓	✓	✓	✓

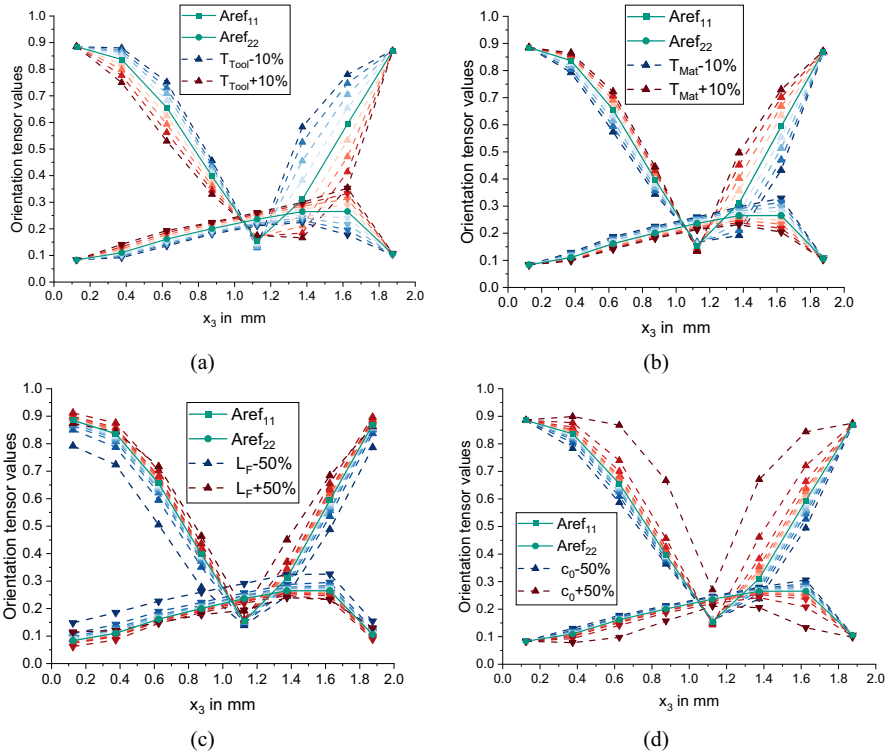

Fig. 3 Fiber orientation results at position P_1 for parameter variation of T_{Tool} (**a**), T_{Mat} (**b**), L_{F} (**c**) and c_0 (**d**). Reference simulation in green, low values in blue, high values in red

rise of T_{Mat} shows a similar influence as a rise of T_{Tool}, but according to our previous work [31] the influence of T_{Tool} and T_{Mat} on the in-mold pressure is also opposite. Rising the temperature lowers the viscosity and benefits the curing reaction (which raises the viscosity), both in a non-linear way. Rising T_{Mat} benefits the curing and therefore rises the viscosity, but the direct influence on the material's viscosity is marginal, since the material is still relatively cold (< 150 °C), this is especially important in the pre-chamber and the sprue, where the surface-to-volume ratio of the mold is low compared to the plate. In the thin plate, T_{Tool} becomes dominant due to the high surface-to-volume ratio and heats the material quickly, lowering the viscosity, much faster than the curing reaction proceeds, which would rise the viscosity. These complex correlations of temperature, curing and resulting viscosity are a typical phenomenon of reactive injection molding [21, 32]. In general, the orientation is more sensitive to T_{Tool} than to T_{Mat} in this case, due the thin-wall character and due to the fact that the absolute variation of T_{Tool} is higher, since the reference value is higher.

The deviations for $c_0 = 0.15$ (+50%) are irregular high compared to the other parameter variations at every point. However, this configuration also results in a high process pressure, and it is questionable if a process would run stable with such a high pre-curing state.

Contrary to the temperatures and curing state, the simulations with fiber length variation show no clear and monotonous influence on the orientation (besides P_1) for longer or shorter fibers. One reason might be, that the fiber length influences the calculated

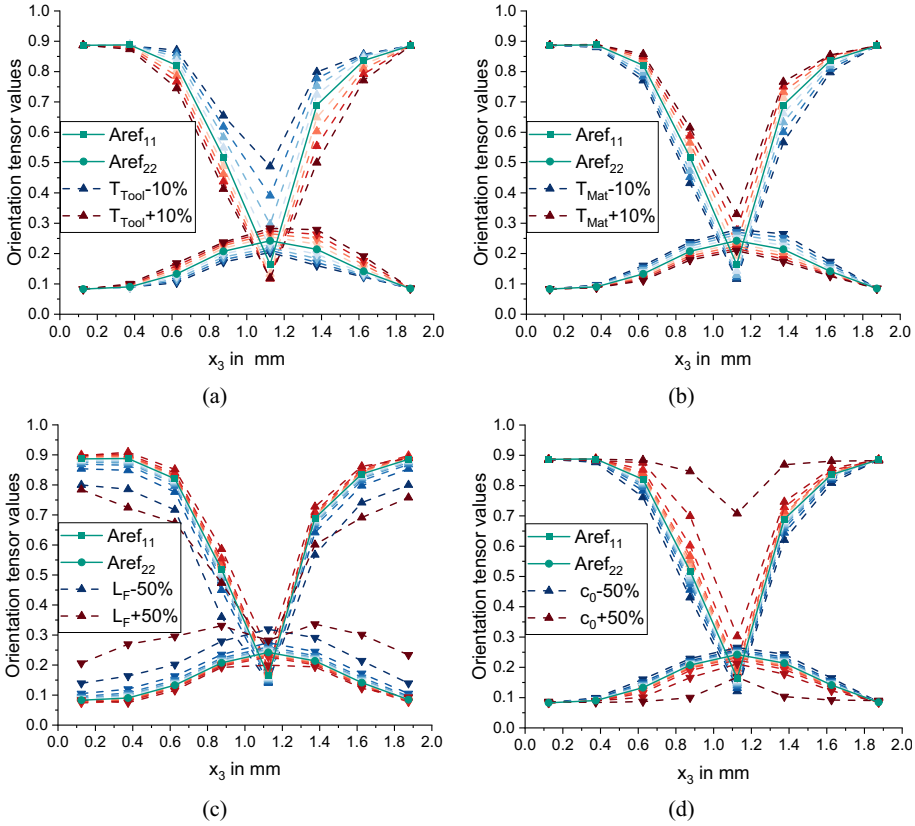

Fig. 4 Fiber orientation results at position P_2 for parameter variation of T_{Tool} (**a**), T_{Mat} (**b**), L_{F} (**c**) and c_0 (**d**). Reference simulation in green, low values in blue, high values in red

orientation in two ways. Firstly, a rise of fiber length leads to a rise of viscosity. But a change of fiber length only affects η_{11} (Eq. (4)), in a non-linear way, while for example c_0 is considered in the matrix viscosity η_{M} (Eq. (5)), which is considered in every parameter in Eq. (4). Therefore, the influence of fiber length variations on the viscosity is more anisotropic, compared to temperature or curing. The other aspect is that the fiber length is directly considered in the orientation evolution equation (Eq. (1)) and the calculation of C_{I} (Eq. (2)). Contrary to temperatures and curing, a variation of fiber length also creates deviations of the orientation state near the wall at every position.

Focusing on P_1, the simulations show a low influence on orientation in the core and near the walls and higher deviations in the layers between core and walls for temperatures and curing. At position P_2 the deviations in the simulation are higher in the core region and quite small near walls. This also applies for P_3 where nearly no deviations are detectable near the walls in simulation. With greater distance from the sprue and therefore longer flow path, the fibers align more and more in their steady-state orientation and influence of temperature and curing becomes less important. This does not apply for L_{F}, which influences the steady-state orientation by the calculation of interaction coefficient C_{I}. Therefore, variations of L_{F} cause higher deviations at P_2 and P_3 also near the walls.

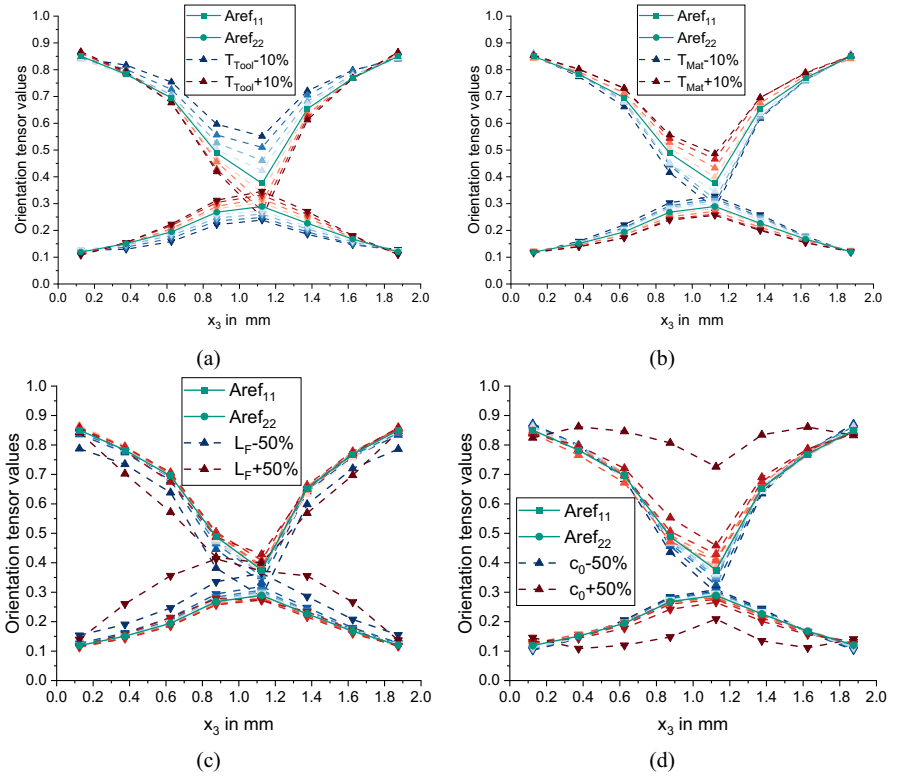

Fig. 5 Fiber orientation results at position P_3 for parameter variation of T_{Tool} (**a**), T_{Mat} (**b**), L_{F} (**c**) and c_0 (**d**). Reference simulation in green, low values in blue, high values in red

3 Approximation Schemes

3.1 Approximation Methods

In this section, four different approaches to approximate the resulting fiber orientation for an arbitrary parameter deviation, based on the results shown in Sect. 2.2.2 are presented. In a first step it is checked if orientation states for variation of single parameters can be approximated by a parameter-space interpolation, so only T_{Tool}, T_{Mat}, L_{F} or c_0 are varied. In a second step, it is checked if a superposition of deviations is possible, so multiple parameters are varied. In general, two approximation schemes are compared. The first one is based on the tensor components of $\boldsymbol{A}$, the second one on its eigenvectors $\boldsymbol{\nu}$ and eigenvalues λ. In case of multiple parameters being varied, the schemes are again separated in two approaches, differing in the point of superposition of the results, which can be done before or after the reconstruction of the orientation state. The approaches are explained in detail in the following sections.

3.1.1 *Parameter-Space Interpolation of Components of A, v and λ for Single Parameter Variations*

The reconstruction of orientation states that are not captured in the parameter variation of Sect. 2.2.2 is performed by interpolating these results. For this purpose, two different schemes are introduced, where interpolated quantities are marked with a $\widetilde{\bullet}$ (for example $\widetilde{\boldsymbol{A}}$). The first scheme is the direct interpolation of the components of $\boldsymbol{A}$ and therefore named Euclidean (euc) in the following. The second scheme is the interpolation of the eigenvectors and eigenvalues of $\boldsymbol{A}$ and therefore called spectral (spec) in the following.

The Euclidean interpolation is defined by

$$\widetilde{\boldsymbol{A}}_{\mathrm{euc}}^{\mathrm{notSPD\_notnorm}} = \mathrm{interp}(\boldsymbol{A}_n, m), \tag{6}$$

where $\boldsymbol{A}_n$ represents the orientation states given in Sect. 2.2.2, hence $n \in \{-50\%, -25\%, -15\%, -10\%, -7.5\%, -5\%, -2.5\%, 2.5\%, 5\%, 7.5\%, 10\%, 15\%, 25\%, 50\%\}$ for L_{F} or c_0 and $n \in \{-10\%, -7.5\%, -5\%, -2.5\%, 2.5\%, 5\%, 7.5\%, 10\%\}$ for T_{Tool} or T_{Mat}. m is the point of interpolation, being $m \in [-50\%, 50\%]$ for L_{F} or c_0 and $m \in [-10\%, 10\%]$ for T_{Tool} or T_{Mat}. The interpolation does not guarantee that the new tensor fulfills the requirements of a second order orientation tensor, like being a symmetric semi-positive definite tensor (SPD) and trace($\boldsymbol{A}$) = 1, therefore it is also indexed with 'notSPD' and 'notnorm'. Hence, it is checked if the reconstructed tensor is SPD and otherwise it is transformed to its nearest semi-positive definite equivalent (using the Frobenius norm as distance metric), so

$$\widetilde{\boldsymbol{A}}_{\mathrm{euc}}^{\mathrm{notnorm}} = \mathrm{nearestSPD}\left(\widetilde{\boldsymbol{A}}_{\mathrm{euc}}^{\mathrm{notSPD\_notnorm}}\right). \tag{7}$$

This procedure is presented by Higham [33], the implementation is provided by D'Errico [34]. Afterwards the tensor is normalized and the final reconstructed tensor is given by

$$\widetilde{\boldsymbol{A}}_{\mathrm{euc}} = \widetilde{\boldsymbol{A}}_{\mathrm{euc}}^{\mathrm{notnorm}} / \|\widetilde{\boldsymbol{A}}_{\mathrm{euc}}^{\mathrm{notnorm}}\|. \tag{8}$$

Alternatively, an orientation tensor can be reconstructed by reconstructing the eigenvectors and eigenvalues,

$$\begin{aligned} \widetilde{\boldsymbol{v}}_k^{\mathrm{notnorm}} &= \mathrm{interp}\left(\boldsymbol{v}_{kn}, m\right) \\ \widetilde{\lambda}_k^{\mathrm{notnorm}} &= \mathrm{interp}(\lambda_{kn}, m) \end{aligned}, \tag{9}$$

with $k \in \{1, 2, 3\}$, since three eigenvectors and three eigenvalues exist. These quantities must also be normalized,

$$\begin{aligned} \widetilde{\boldsymbol{v}}_k &= \frac{\widetilde{\boldsymbol{v}}_k^{\mathrm{notnorm}}}{\|\widetilde{\boldsymbol{v}}_k^{\mathrm{notnorm}}\|} \\ \widetilde{\lambda}_k &= \frac{\widetilde{\lambda}_k^{\mathrm{notnorm}}}{\left|\sum_{k=1}^{3} \widetilde{\lambda}_k^{\mathrm{notnorm}}\right|}. \end{aligned} \tag{10}$$

The orientation tensor $\widetilde{\boldsymbol{A}}_{\mathrm{spec}}$ can be reconstructed with $\widetilde{\boldsymbol{v}}_k$ and $\widetilde{\lambda}_k$, where also Eq. (7) and Eq. (8) are applied to guarantee that $\widetilde{\boldsymbol{A}}_{\mathrm{spec}}$ is SPD and trace($\widetilde{\boldsymbol{A}}_{\mathrm{spec}}$) = 1.

3.1.2 Superposition of Approximations for Multi-dimensional Parameter-space Interpolation

The aim of this work is to approximate fiber orientation states due to variations in a multi-dimensional parameter space fast and efficiently. Therefore, this Section presents two approaches to superpose reconstructed orientation stages of single parameter variations, explained in Sect. 3.1.1.

The first approach is to simply average (index av) the reconstructed orientation tensors, so

$$\widetilde{\boldsymbol{A}}^{\text{all\_notSPD\_notnorm}}_{\text{euc\_av}} = {}^{1}\!/_{4}\left(\widetilde{\boldsymbol{A}}^{\text{T}_{\text{Tool}}}_{\text{euc}} + \widetilde{\boldsymbol{A}}^{\text{T}_{\text{Mat}}}_{\text{euc}} + \widetilde{\boldsymbol{A}}^{\text{L}_{\text{F}}}_{\text{euc}} + \widetilde{\boldsymbol{A}}^{c_0}_{\text{euc}}\right), \tag{11}$$

and

$$\widetilde{\boldsymbol{A}}^{\text{all\_notSPD\_notnorm}}_{\text{spec\_av}} = {}^{1}\!/_{4}\left(\widetilde{\boldsymbol{A}}^{\text{T}_{\text{Tool}}}_{\text{spec}} + \widetilde{\boldsymbol{A}}^{\text{T}_{\text{Mat}}}_{\text{spec}} + \widetilde{\boldsymbol{A}}^{\text{L}_{\text{F}}}_{\text{spec}} + \widetilde{\boldsymbol{A}}^{c_0}_{\text{spec}}\right). \tag{12}$$

The index 'all' indicates that all four parameters are varied for the reconstruction of this orientation tensor. Again, Eq. (7) and Eq. (8) are subsequently applied to guarantee that the reconstructed tensors represent admissible orientation states and gain the final $\widetilde{\boldsymbol{A}}^{\text{all}}_{\text{euc\_av}}$ and $\widetilde{\boldsymbol{A}}^{\text{all}}_{\text{spec\_av}}$.

The second approach is to first calculate the individual changes to the reference case due to single parameter deviation, sum up these changes and add them to the orientation state of the reference case to get the new orientation state. Hence, the individual deviations $\Delta\widetilde{\boldsymbol{A}}^{i}$ are defined as

$$\Delta\widetilde{\boldsymbol{A}}^{i} = \text{interp}\left(\boldsymbol{A}^{i}_{n}, m\right) - \boldsymbol{A}_{\text{ref}}, \tag{13}$$

where the index 'ref' represents the reference case and $i \in \{T_{\text{Tool}}, T_{\text{Mat}}, L_{\text{F}}, c_0\}$. The absolute deviation due to all parameters is given by

$$\Delta\widetilde{\boldsymbol{A}}^{\text{abs}} = \Delta\widetilde{\boldsymbol{A}}^{\text{T}_{\text{Tool}}} + \Delta\widetilde{\boldsymbol{A}}^{\text{T}_{\text{Mat}}} + \Delta\widetilde{\boldsymbol{A}}^{\text{L}_{\text{F}}} + \Delta\widetilde{\boldsymbol{A}}^{c_0} \tag{14}$$

And the reconstructed orientation state based on adding $\Delta\widetilde{\boldsymbol{A}}^{\text{abs}}$ (index 'added') is given by

$$\widetilde{\boldsymbol{A}}^{\text{all\_notSPD\_notnorm}}_{\text{euc\_added}} = \boldsymbol{A}_{\text{ref}} + \Delta\widetilde{\boldsymbol{A}}^{\text{abs}}. \tag{15}$$

Again Eq. (7) and Eq. (8) are applied to guarantee that the reconstructed tensor represents an admissible orientation state and gain the final $\widetilde{\boldsymbol{A}}^{\text{all}}_{\text{euc\_added}}$.

Similarly, this procedure is performed for $\boldsymbol{\nu}_k$ and λ_k, so

$$\begin{aligned} \Delta\widetilde{\boldsymbol{\nu}}^{i}_{k} &= \text{interp}\left(\boldsymbol{\nu}^{indi}_{kn}, m\right) - \boldsymbol{\nu}^{\text{ref}}_{k} \\ \Delta\widetilde{\lambda}^{i}_{k} &= \text{interp}\left(\lambda^{indi}_{kn}, m\right) - \lambda^{\text{ref}}_{k} \end{aligned} \tag{16}$$

and

$$\begin{aligned} \Delta\widetilde{\boldsymbol{\nu}}^{\text{abs}}_{k} &= \Delta\widetilde{\boldsymbol{\nu}}^{\text{T}_{\text{Tool}}}_{k} + \Delta\widetilde{\boldsymbol{\nu}}^{\text{T}_{\text{Mat}}}_{k} + \Delta\widetilde{\boldsymbol{\nu}}^{\text{L}_{\text{F}}}_{k} + \Delta\widetilde{\boldsymbol{\nu}}^{c_0}_{k} \\ \Delta\widetilde{\lambda}^{\text{abs}}_{k} &= \Delta\widetilde{\lambda}^{\text{T}_{\text{Tool}}}_{k} + \Delta\widetilde{\lambda}^{\text{T}_{\text{Mat}}}_{k} + \Delta\widetilde{\lambda}^{\text{L}_{\text{F}}}_{k} + \Delta\widetilde{\lambda}^{c_0}_{k} \end{aligned} \tag{17}$$

as well as

$$\begin{aligned} \widetilde{\boldsymbol{\nu}}_k^{\text{added\_notnorm}} &= \boldsymbol{\nu}_k^{\text{ref}} + \Delta\widetilde{\boldsymbol{\nu}}_k^{\text{abs}} \\ \widetilde{\lambda}_k^{\text{added\_notnorm}} &= \lambda_k^{\text{ref}} + \Delta\widetilde{\lambda}_k^{\text{abs}} \end{aligned} . \tag{18}$$

Subsequently, Eq. (10) is applied on $\widetilde{\boldsymbol{\nu}}_k^{\text{added\_notnorm}}$ and $\widetilde{\lambda}_k^{\text{added\_notnorm}}$ and $\widetilde{\boldsymbol{A}}_{\text{spec\_added}}^{\text{all}}$ can be build with $\widetilde{\boldsymbol{\nu}}_k^{\text{added}}$ and $\widetilde{\lambda}_k^{\text{added}}$ and Eq. (7) and Eq. (8) are applied.

3.2 Quantities to evaluate the approximation quality

The four different approximation approaches presented in Sect. 3.1 can be verified by comparing them to a full 3D process simulation, performed with the parameters for T_{Tool}, T_{Mat}, L_{F} and c_0 also used in the interpolation. To ensure that the approximation is valid on the whole domain, multiple points along the plate surface and over the plate thickness are compared.

Since the orientation tensor contains 6 different values, which are compared at eleven positions containing 8 cells, a full comparison would include 528 samples, which is hard to illustrate. Furthermore, a direct comparison of tensor components is not representative [19]. Therefore, scalar and dimensionless quantities are defined to compare the orientation tensors with respect to shape and direction.

To compare the shape, the fractional anisotropy (FA) is considered. This quantity is defined as

$$FA = \sqrt{\frac{3\left(\lambda_1 - \widehat{\lambda}\right)^2 + \left(\lambda_2 - \widehat{\lambda}\right)^2 + \left(\lambda_3 - \widehat{\lambda}\right)^2}{2\left(\lambda_1^2 + \lambda_2^2 + \lambda_3^2\right)}}, \tag{19}$$

with $\widehat{\lambda} = \left(\lambda_1 + \lambda_2 + \lambda_3\right)/3 = 1/3$. It is $FA \in [0,1]$, where 0 means isotropic orientation, and 1 represents unidirectional oriented fibers [16]. Therefore, FA represents the degree of anisotropy without correspondence to the direction of the tensor or a coordinate system.

To compare FA_{apx}, calculated with the reconstruction schemes explained in Sect. 3.1, with FA_{sim} of a full 3D-simulation with identical parameters, the measure FA_{comp} is defined by

$$FA_{\text{comp}} = \begin{cases} {FA_{\text{apx}}}/{FA_{\text{sim}}} & \text{for } FA_{\text{sim}} \geq FA_{\text{apx}} \\ {FA_{\text{sim}}}/{FA_{\text{apx}}} & \text{for } FA_{\text{sim}} < FA_{\text{apx}} \end{cases} . \tag{20}$$

Hence, $FA_{\text{comp}} \in [0,1]$, with $FA_{\text{comp}} = 1$, if $FA_{\text{apx}} = FA_{\text{sim}}$, and FA_{comp} becomes smaller for higher deviations between FA_{apx} and FA_{sim}.

Besides the shape, also the direction of the fiber orientation tensors is compared. Therefore, the eigenvector, corresponding to the highest eigenvalue $\boldsymbol{\nu}_3$ is regarded, representing the principal direction of the tensor. If the reconstructed eigenvector $\boldsymbol{\nu}_3^{\text{apx}}$ and the simulated eigenvector $\boldsymbol{\nu}_3^{\text{sim}}$ are identical, it is $\left|\boldsymbol{\nu}_3^{\text{apx}} \bullet \boldsymbol{\nu}_3^{\text{sim}}\right| = 1$. Similar to FA_{comp}, the values become smaller, if the angle between $\boldsymbol{\nu}_3^{\text{apx}}$ and $\boldsymbol{\nu}_3^{\text{sim}}$ becomes higher. So, the value for direction comparison $EV_{\text{comp}} \in [0,1]$ is defined as

$$EV_{\text{comp}} = \left|\boldsymbol{\nu}_3^{\text{apx}} \cdot \boldsymbol{\nu}_3^{\text{sim}}\right|. \tag{21}$$

4 Approximation Results and Discussion

In this section, the results of the reconstruction of orientation tensors for different parameter variations and different reconstruction schemes are presented and discussed. At first, the considered parameter variations are explained (Sect. 4.1). In Sect. 4.2, single parameters are varied and the reference case is reconstructed to verify the general procedure. Additionally, different interpolation intervals are compared to quantify the needed number of input simulations for the reconstruction. Sections 4.3 and 4.4 compare the results for multiple parameter changes. In Sect. 4.6, probabilistic data with random input is created fast and efficiently.

4.1 Parameter Variations and Labeling Conventions

In the following sections, the simulated and reconstructed cases are named according to a specific scheme to contain all relevant information. This scheme is *Parameter – deviation in percent*. The *Parameters* are T_{Tool} (Tt), T_{Mat} (Tm), L_{F} (FL) and initial degree of cure (c). Hence, if for example, all parameters are varied by + 5%, the case is named *Tt5Tm5FL5c5*. If the reference case is reconstructed and only one parameter is interpolated, for example the Euclidean interpolation of T_{Tool}, the case is named T_{Tool} *euc*.

At first, the reconstruction of orientation is done by parameter-space interpolation to the reference case for every parameter individually, either by Euclidean or by spectral interpolation. These results are also used to determine threshold interval sizes, needed to create acceptable results. Afterwards 3 different parameter variations, all reconstructed Euclidean or by eigenvectors and eigenvalues as well es by adding or by average are regarded. The values of the parameter deviations (with respect to the reference case) are given in Table 2.

The following cases represent a low deviation for all parameters (Tt5Tm5FL5c5) and a high deviation for all parameters (Tt10Tm-10FL50c-50) to generally determine if a superposition of multiple parameter variations creates meaningful results. Finally, a completely randomly configuration (Tt8.15Tm1.23FL-31.61c13.93) is regarded, so interpolation is needed to reconstruct the orientation.

4.2 Results for Reference Case and Interval Evaluation

This section presents the results of FA_{comp} (Fig. 6) and EV_{comp} (Fig. 7) if only one parameter is varied. FA_{comp} and EV_{comp} are determined in every element at every Positions P_1 to P_{11} and the shown results are the average of these individual values. Euclidian and spectral interpolation for reconstruction of the orientation tensors are compared. Furthermore, different interval sizes for interpolation are compared, where the deviation

Table 2 Names and parameter deviations of the reconstructed cases for comparison to simulation

Name	Deviation in %			
	T_{Tool}	T_{Mat}	L_{F}	c_0
'Parameter' euc/spec	0.00	0.00	0.00	0.00
Tt5Tm5FL5c5	5.00	5.00	5.00	5.00
Tt10Tm-10FL50c-50	10.00	-10.00	50.00	-50.00
Tt8.15Tm1.23FL-31.61c13.93	8.15	1.23	-31.61	13.93

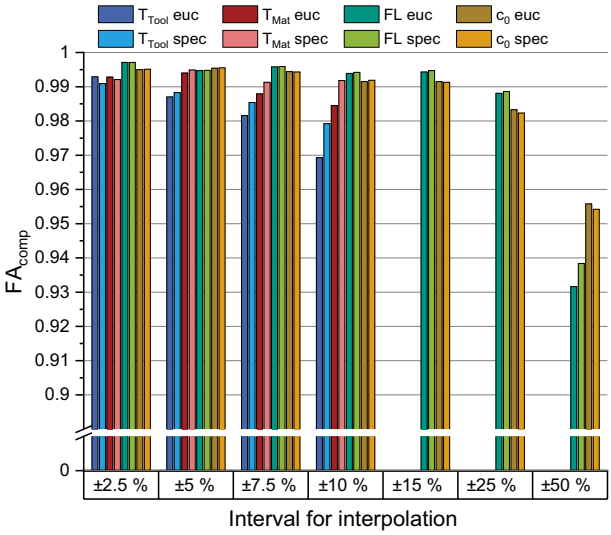

Fig. 6 Averaged values of FA_{comp} for different single parameter variations with Euclidian and spectral reconstruction. Different interval sizes for reconstruction of the reference case (0%). Average for all evaluation points (cf. Fig. 2)

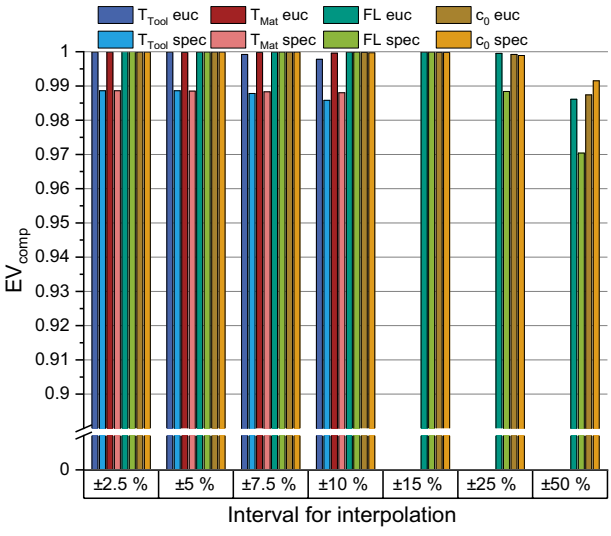

Fig. 7 Averaged values of EV_{comp} for different single parameter variations with Euclidian and spectral reconstruction. Different interval sizes for reconstruction of the reference case (0%). Average for all evaluation points (cf. Fig. 2)

windows of the simulations used for reconstruction are indicated as different groups in Fig. 6 and Fig. 7. For example, in the group ±2.5%, the simulation results of the -2.5% and +2.5% simulations are used for the parameter-space interpolation and reconstruction of the reference case, while in the group ±10%, the simulation results of the -10% and +10% simulations are used. The groups ±15%, ±25% and ±50% only contain results for L_F and c_0, since the temperatures have been varied only up to ±10% (cf. Table 1). The results in Fig. 6 and Fig. 7 present the average for all eleven evaluation points.

The results generally show that a reconstruction of orientation tensors due to parameter changes is possible, with FA_{comp}>0.93 and EV_{comp}>0.97 for every case. Therefore, adequate results can be achieved via parameter-space interpolation, even

if the simulations used for interpolation show high deviations from the reconstructed configuration.

For larger interpolation intervals, the spectral method creates better results for FA_{comp} for all varied parameters, except for c_0 ±25% and ±50%. This result is expected, since the spectral method should capture the shape of the tensor better, especially in case of higher deviations and FA_{comp} indicates the quality of the shape of the reconstructed tensor. For only ±2.5% variations, the FA_{comp} results of the spectral method are slightly worse. Since the deviations here are very small, the Euclidian method creates good results, while the spectral method shows small numerical error due to more normalization steps.

Regarding EV_{comp} (Fig. 7) the spectral method creates worse results in most cases, where again the additional normalization steps may be a reason. However, the quality of the principal direction of the interpolated tensor is good with EV_{comp}=0.97 being the lowest value in case of spectral reconstruction for a fiber length interval of ±50%.

4.3 Results at the Evaluation Points for Multiple Parameter Variations

Figure 8 and Fig. 9 show the results of FA_{comp} and EV_{comp} for the evaluation positions P_1 to P_{11}, where FA_{comp} and EV_{comp} are determined in every element and the shown results are the average for all 8 elements over plate thickness. All simulation data presented in

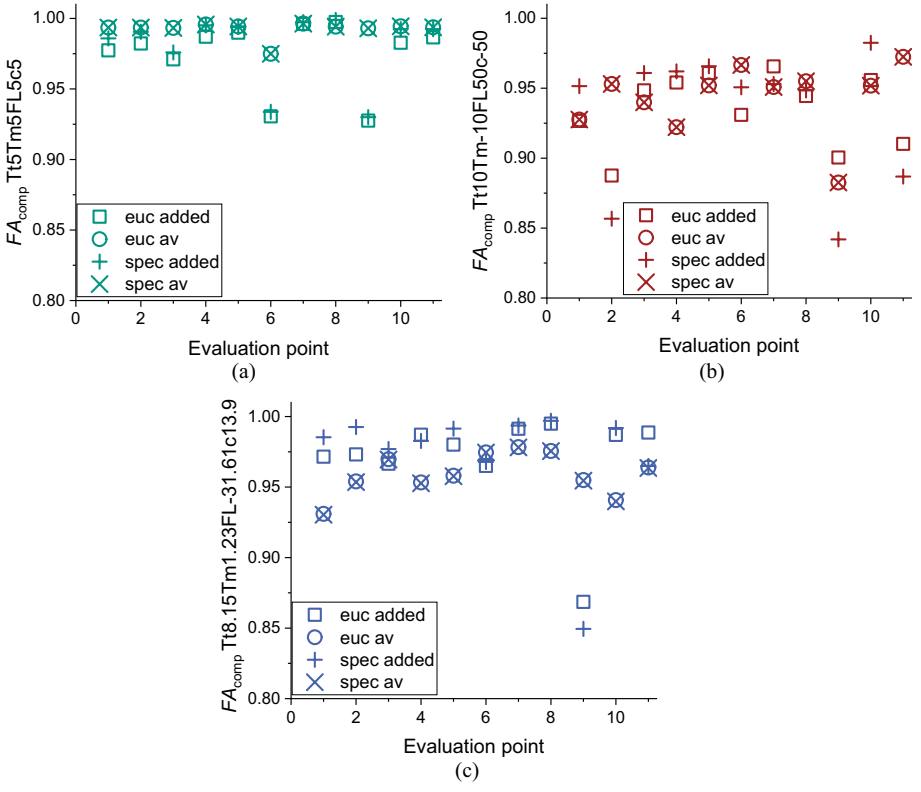

Fig. 8 Averaged values of FA_{comp} at the evaluation points P_1 to P_{11} (cf. Fig. 2). **a**-**c** represent the different parameter configurations according to Table 2

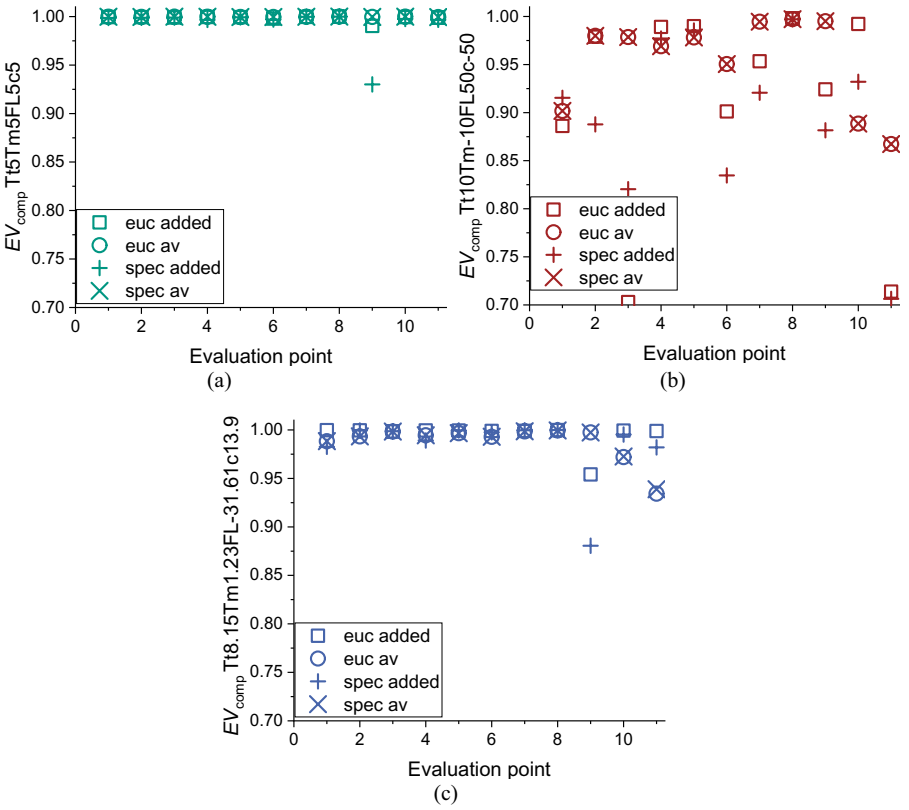

Fig. 9 Averaged values of EV_{comp} at the evaluation points P_1 to P_{11} (cf. Fig. 2). **a**-**c** represent the different parameter configurations according to Table 2

Sect. 2.2 is used for the multi-dimensional parameter-space interpolation. The reconstructed results are compared to full 3D-simulations, performed with the corresponding parameter configuration. In both cases (FA_{comp} and EV_{comp}), the results of the averaging method are quite identical, independent of the reconstruction being direct (euc) or with eigenvectors and eigenvalues (spec).

On the opposite, the two adding methods create different results, where the spectral method often creates the worst results. Apart from the configuration Tt10Tm-10FL50c-50 (largest parameter variations, cf. Fig. 8b), the averaging methods create results with FA_{comp} and EV_{comp}>0.9 at every evaluation point, while the adding method still creates results with FA_{comp} and EV_{comp}>0.85. The good results for Tt5Tm5FL5c5 (Fig. 8a and Fig. 9a) show that a superposition of small individual changes creates meaningful results when orientation tensors are reconstructed. This applies to all presented schemes, although the averaging method creates better results than the adding method. Furthermore, the good results for Tt8.15Tm1.23FL-31.61c13.9 (Fig. 8c and Fig. 9c) show that a reconstruction by superposition is possible even if the individual orientation tensors (or orientation changes) are built by a parameter-space interpolation. Thus, a multi-dimensional parameter-space interpolation creates meaningful results.

Here, the adding method creates better results, but with outliers, while the averaging approach shows a more constant quality between the different evaluation points.

For Tt10Tm-10FL50c-50, the results are slightly worse at P_9 to P_{11}, but still > 0.86, when the averaging method is used. The worst results are often at P_6, P_9 and P_{11}, being the evaluation points near the end of the flow path and therefore critical in fiber orientation and positions with higher uncertainty also in the real process. Comparing the adding approach over all parameter configurations, the spectral method often creates better results than the Euclidian approach in case of FA_{comp} and vice versa for EV_{comp}, especially for higher parameter variations. This fits to the results of Sect. 4.2 and supports the statement, that the spectral method is more suitable to capture the shape of the reconstructed tensor.

4.4 *Results at Exemplary Evaluation Point P_2 for Multiple Parameter Variations Over Plate Thickness*

To illustrate if the interpolation approach is able to predict fiber orientation over plate thickness, being important to model the bending behavior of the plate accurately, the results of FA_{comp} and EV_{comp} are shown in Fig. 10 over plate thickness at evaluation point P_2 for the two cases Tt10Tm-10FL50c-50 (red) and Tt8.15Tm1.23FL-31.61c13.9 (blue). This illustration is chosen exemplarily to show the results over plate thickness, since the illustration of all cases and evaluation points is not illustratable within a compact amount of space. The two cases Tt10Tm-10FL50c-50 and Tt8.15Tm1.23FL-31.61c13.9 are chosen, since they represent the case with the highest deviations and the case with interpolation and superposition of orientation states. The point P_2 is chosen, since it is in the middle of the plate and therefore a representative region.

The approximation of Tt10Tm-10FL50c-50 shows the worst results due to the high parameter variation and the adding approaches create higher deviations at most points. It is $FA_{\text{comp}} > 0.75$ and $EV_{\text{comp}} > 0.9$ for Tt10Tm-10FL50c-50 (besides one outlier at 1.375 mm) as well as $FA_{\text{comp}} > 0.83$ and $EV_{\text{comp}} > 0.97$ for Tt8.15Tm1.23FL-31.61c13.9 in every case. Considering both deviation cases, the averaging approaches create better results, while the adding approaches create higher deviations, especially in the core region

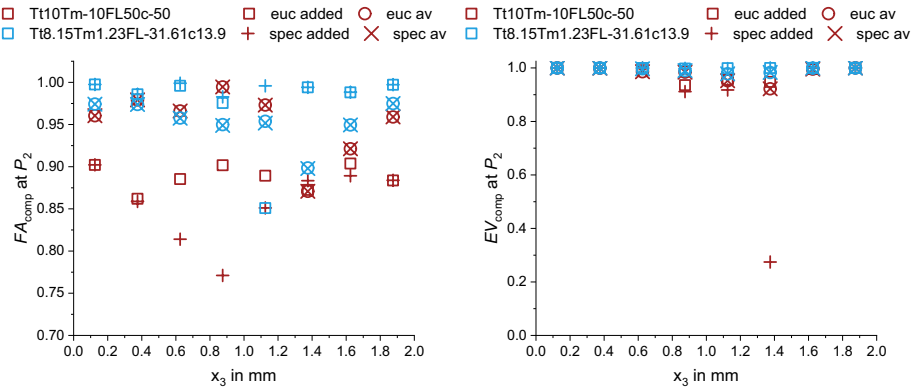

Fig. 10 Values of FA_{comp} (**a**) and EV_{comp} (**b**) for configuration Tt10Tm-10FL50c-50 (red) and Tt8.15Tm1.23FL-31.61c13.9 (blue) at the evaluation point P_2 over plate thickness

(0.5 mm < x_3 < 1.5 mm). The results of FA_{comp} and especially EV_{comp} are better at the surface regions of the plate (x_3 < 0.5 mm and x_3 > 1.5 mm), which is important in context of modeling bending deformations. In summary, all approaches but especially the averaging approaches are capable of predicting the uncertainty fiber orientation due to variation of T_{Tool}, T_{Mat}, L_F and c_0 accurately, also over plate thickness.

4.5 Results at the Evaluation Points for Multiple Parameter Variations with Larger Interpolation Intervals

In the following, the results for Tt5Tm5FL5c5 (Fig. 11) and Tt8.15Tm1.23FL-31.61c13.9 (Fig. 12) are reconstructed from large-interval simulations only, i.e. from T_{Tool} and T_{Mat} with ± 10% and L_F and c_0 with ± 50%. These large-interval results (light-green in Fig. 11 and light-blue in Fig. 12) are compared to the results from Sect. 4.3, where all data has been used for interpolation (all-data results, dark-green and dark-blue). For the reconstruction of Tt5Tm5FL5c5 with all data (Fig. 11, dark-green), only superposition, but no interpolation is necessary. Therefore, the difference between the all-data case and the large-interval case highlights the influence of the interpolation of the large-interval case (light-green), when superimposing multiple parameter changes. Of course, the results of the large interval are worse, but in an acceptable range, with FA_{comp}>0.85 and EV_{comp}>0.9 for the adding approach and even FA_{comp}>0.95 and EV_{comp}>0.975 for the averaging approach. Again, the spectral method (combined with averaging) creates the best results for FA_{comp}. For EV_{comp} the results of the spectral and Euclidian approach (with averaging) are quite similar.

For the reconstruction of Tt8.15Tm1.23FL-31.61c13.9 (Fig. 12), both the all-data results and the large-interval results are calculated with a multi-dimensional parameter-space interpolation. While for the all-data set the adding approaches create better results, the averaging method creates better results for the large interval. It is FA_{comp} >0.8 and EV_{comp}>0.85 at every point for the adding approaches and even FA_{comp} >0.9 and EV_{comp}>0.925 for the averaging approaches. This again highlights that a

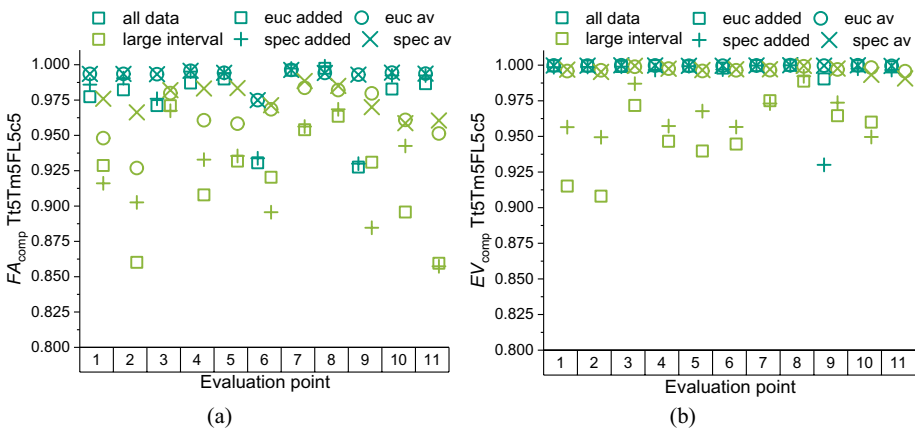

Fig. 11 Averaged values of FA_{comp} (**a**) and EV_{comp} (**b**) for configuration Tt5Tm5FL5c5 at the evaluation points P_1 to P_{11} with different interval sizes for interpolation

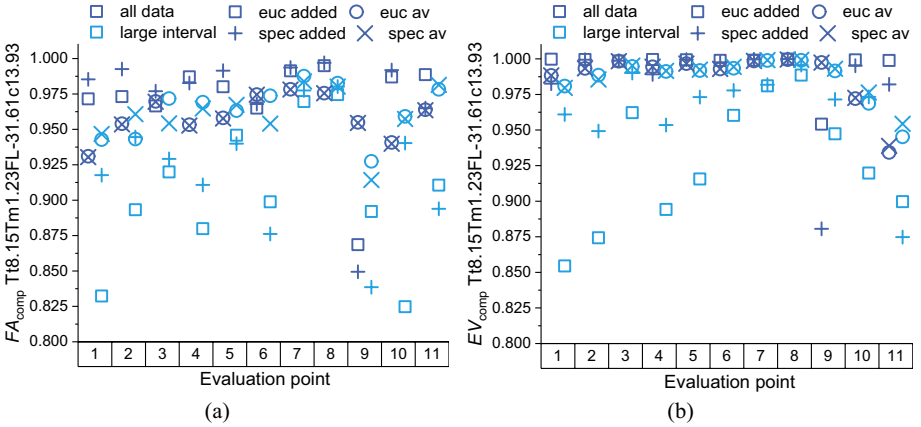

Fig. 12 Averaged values of FA_{comp} (**a**) and EV_{comp} (**b**) for configuration Tt8.15Tm1.23FL-31.61c13.93 at the evaluation points P_1 to P_{11} with different interval sizes for interpolation

reconstruction of orientation by interpolation of multiple parameter variations creates meaningful results, even if large intervals are chosen for the interpolation, so only a few full 3D-simulations are needed as input.

In summary, all four presented schemes are able to approximate the shape and direction of orientation tensors for multiple parameter variations. So, in general it is possible to interpolate second-order orientation tensors in a multi-dimensional parameter space, even if the deviations are high and the intervals are large. In most cases the averaging method (Eq. (11) and Eq. (12)) creates the best results, especially in case of large intervals. Here the results of Euclidean interpolation of tensor values and the results of spectral interpolation of eigenvectors and eigenvalues are often quite similar for EV_{comp}, while the spectral interpolation creates better results for FA_{comp} in most cases, especially when using large intervals. Therefore, ongoing approximations will be performed with the spectral averaging approach.

To quantify the impact of a value like $EV_{comp} = 0.939$, being the maximum deviation for the spectral averaging approach in the Tt8.15Tm1.23FL-31.61c13.93 case, on the structural properties, the work of Maertens [30] is considered. In [30] circular specimens are extracted from identical material and identical plates as in this study, except that the plates for the specimens have a thickness of 4 mm. Tensile tests under different angles are performed with these specimens to characterize the anisotropy of the material. $EV_{comp} = 0.939$ refers to an angle of about 20°. The maximum change of Young's modulus in [30] for an interval of 20° ranges from 1.68 GPa to 1.6 GPa, being a change of 0.08 GPa, or 4.76%. Of course, this only is valid for the considered material system and numerical and experimental results. A holistic influence of the approximation error on the prediction of mechanical properties can hardly be quantified, since it depends on material properties, approaches for homogenization and closure approximation for $\mathbb{A}$, which are necessary for modeling the anisotropic behavior of discontinuous FRPs.

Unlike spatial interpolation, no weighting factors are used in the multi-dimensional parameter-space interpolations presented here, since there is no physical meaning to weight the four parameters T_{Tool}, T_{Mat}, L_F and c_0 to each other.

4.6 Orientation Approximation with Probabilistic Parameter Variation

In this Section, the spectral interpolation method with averaging superposition of different parameter variations (spec av method) will be used to create 100 orientation state approximations, with random variation of the parameters T_{Tool}, T_{Mat}, L_{F} and c_0. For the four parameters, a uniform distribution for the range given in Table 1 is assumed. The results are evaluated at the positions P_1, P_2 and P_3 (cf. Fig. 2). The results are given in Fig. 13.

The 3D-simulation with reference values (green) and the average of the approximations (blue) fit well, verifying the approximation, since the average should be the reference case, where the deviations of the parameters are all zero. Uniform distributions of the input parameters do not lead to a uniform distribution of orientation, visible in the range of results of the approximation (blue shading) being unsymmetric, as detectable in the core region at P_2 and P_3. Often, the lowest value of A_{11} is closer to the average than the highest value, which fits to the results of the 3D-simulations, shown in Fig. 3 to Fig. 5. The approximations represent correct tendencies, predicting a higher uncertainty

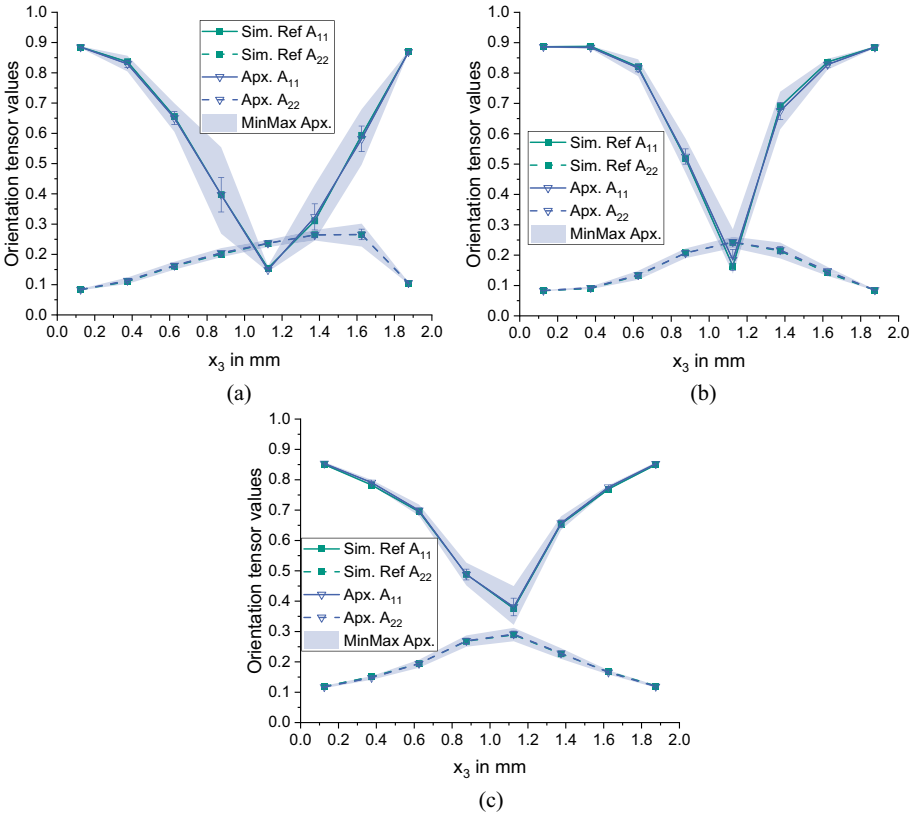

Fig. 13 Components of the second order fiber orientation tensor over plate thickness at position P_1 (**a**), P_2 (**b**) and P_3 (**c**) with corresponding 3D simulation result (green, squares) and approximation with standard deviation. Average of the 100 approximation (blue, triangles) and range of the approximations (blue shading)

in the core region of P_2 and P_3 and a smaller uncertainty in the core region of P_1 for A_{11}, which fits to the results shown in Sect. 2.2.2. Accordingly, the uncertainty is smaller near the walls of P_2 and P_3.

The creation of 100 approximations was performed for all eleven points P_1 to P_{11} and took about 10 s on a normal working laptop. Thus, computing 100 orientation states for the complete plate (in every element) would take less than 8 h, while one full 3D process simulation takes about 4 h on a 16-core workstation. This highlights how fast and efficient the approximation is working. It can be applied on the whole simulation domain (not only the eight elements over plate thickness at P_1 to P_{11}) and can predict various orientation variations for the complete part.

In summary, the interpolation-based approximation approach is able to predict the uncertainty of orientation states due to individual variation of multiple parameters within a wide range. Although there is a high level of simplification and the efficiency of the approach, the results are in good agreement with 3D-simulations. It should be mentioned that the size of parameter variation, being crucial for uncertainty quantification, is not based on experimental data yet and should be further investigated in future works. However, the aim of this work is to efficiently model the uncertainty by fast approaches, able to fit to 3D-simulation results with equal parameters.

5 Conclusion

Different approaches are presented to approximate the final fiber orientation state in injection molded parts for uncertain manufacturing conditions. To analyze uncertainty, variations of material and tool temperature, fiber length and initial curing state are considered. The approximation approaches are based on a multi-dimensional parameter-space interpolation of beforehand performed 3D-simulations, where the single parameters are varied in specific steps. The approaches differ in the interpolation method (based either on orientation tensor components or on components of the eigenvectors and eigenvalues) and in the superposition of multiple parameter variations (either summing up the parameter-specific offsets or averaging the parameter-specific resulting orientation tensors). The approximations fit well to full 3D-simulations for certain parameter variations in a wide range of parameter values, even if the interpolation intervals are large, which means, that only a few input simulations are needed to create good results. Hence, the interpolation of fiber orientation tensors in a multi-dimensional parameter space is possible and creates meaningful results. In general, averaging the tensors creates better results than adding the offsets. Due to the simple interpolation approach, the approximation can create huge amounts of data efficiently and without the use of weighting factors.

The approximation approach represents a first step to efficiently model the process- and material-induced uncertainty of fiber orientations, being crucial for the thermo-mechanical behavior of the final part. The approach is able to predict the fiber orientation state due to variable input parameters efficiently and with the need of only a few simulations as input. Continuing this idea, the probability distribution of fiber orientations due to uncertain process and material parameters can be determined, if the distribution functions of the input parameters is known. Further investigation is needed to quantify these input uncertainties in the real process.

Although the results of approximation and simulation fit well, the scheme is only a first step. The geometry considered in this study is a simple plate and more complex geometries

should be considered to verify that the approach is able to predict orientation uncertainties in real parts. This includes in particular geometries with many changes of flow direction and thicker wall sections, where the flow is not as shear dominated as it is in the plate in this work. Extending the approach to long fiber materials raises the aspect of fiber breakage modeling, since the fiber length has crucial impact on the orientation interpolation in parameter space. Furthermore, the variation of parameters is comparatively simple, since no variation in time and coordinates is considered so far. The efficiency of the approximation may be further improved by combining the multi-dimensional parameter-space interpolation with a spatial interpolation, so the approximation for a complete part does not need to be performed in every element.

Acknowledgements We would like to thank the 'Deutsche Forschungsgemeinschaft' (DFG) for funding the research project 'MeproSi' (project number: 464119659), which enabled this work. The work is also part of the Heisenberg project "Digitalization of fiber-reinforced polymer processes for resource-efficient manufacturing of lightweight components", funded by DFG (project no. 455807141).

Author Contributions Florian Wittemann performed the major part of the work in terms of method development and implementation. He also wrote the first draft of the paper. Constantin Krauß and Luise Kärger supervised the method development, supported the discussion of simulation results and thoroughly revised the paper.

Funding Open Access funding enabled and organized by Projekt DEAL. This work was enabled by the 'Deutsche Forschungsgemeinschaft' (DFG) by funding the research project 'MeproSi' (project number: 464119659). The work is also part of the Heisenberg project "Digitalization of fiber-reinforced polymer processes for resource-efficient manufacturing of lightweight components", also funded by DFG (project no. 455807141).

Data Availability No datasets were generated or analysed during the current study.

Declarations

Declaration of Generative AI and AI-assisted technologies in the writing process The authors did not use generative AI and AI-assisted technologies in the writing process.

Competing Interests The authors declare no competing interests.

References

1. Tamil, J., Ore, S.H., Gan, K.Y., Ore, S.H., Gan, K.Y., Bo, Y.Y., Ng, G., Wah, P.T., Suthiwongsunthorn, N., Chungpaiboonpatana, S.: Molding flow modeling and experimental study on void control for flip chip package panel molding with molded underfill technology. Int. Symp. Microelectron. **2011**(1), 673–682 (2011). https://doi.org/10.4071/isom-2011-WP1-Paper4
2. Ospald, F.: Numerical simulation of injection molding using openFOAM. Proc. Appl. Math. Mech. **14**(1), 673–674 (2014). https://doi.org/10.1002/pamm.201410320

3. Wittemann, F., Maertens, R., Bernath, A., Hohberg, M., Kärger, L., Henning, F.: Simulation of reinforced reactive injection molding with the finite volume method. J. Compos. Sci. **2**(1), 5 (2018). https://doi.org/10.3390/jcs2010005
4. Wittemann, F., Maertens, R., Kärger, L., Henning, F.: Injection molding simulation of short fiber reinforced thermosets with anisotropic and non-Newtonian flow behavior. Compos. A Appl. Sci. Manuf. **124**, 105476 (2019). https://doi.org/10.1016/j.compositesa.2019.105476
5. Wittemann, F., Kärger, L., Henning, F.: Theoretical approximation of hydrodynamic and fiber-fiber interaction forces for macroscopic simulations of polymer flow process with fiber orientation tensors. Compos. Part C: Open Access **132**(53), 100152 (2021). https://doi.org/10.1016/j.jcomc.2021.100152
6. Wittemann, F., Kärger, L., Henning, F.: Influence of fiber breakage on flow behavior in fiber length- and orientation-dependent injection molding simulations. J. Nonnewton. Fluid Mech. **310**, 104950 (2022). https://doi.org/10.1016/j.jnnfm.2022.104950
7. Karl, T., Zartmann, J., Dalpke, S., Gatti, D., Frohnapfel, B., Böhlke, T.: Influence of flow–fiber coupling during mold-filling on the stress field in short-fiber reinforced composites. Comput. Mech. **71**(5), 991–1013 (2023). https://doi.org/10.1007/s00466-023-02277-z
8. Advani, S.G., Tucker, C.L.: The use of tensors to describe and predict fiber orientation in short fiber composites. J. Rheol. **31**(8), 751–784 (1987). https://doi.org/10.1122/1.549945
9. Cross, M.M.: Rheology of non-newtonian fluids: a new flow equation for pseudoplastic systems. J. Colloid Sci. **20**(5), 417–437 (1965). https://doi.org/10.1016/0095-8522(65)90022-X
10. Castro, J.M., Macosko, C.W.: Studies of mold filling and curing in the reaction injection molding process. Am. Inst. Chem. Eng. J. **28**(2), 250–260 (1982). https://doi.org/10.1002/aic.690280213
11. Meyer, N.: Mesoscale simulation of the mold filling process of sheet molding compound. Doctoral Thesis, Karlsruhe, Germany (2021) https://doi.org/10.5445/KSP/1000143703
12. Jansen, K.M.B., van Dijk, D.J., Husselman, M.H.: Effect of processing conditions on shrinkage in injection molding. Polym. Eng. Sci. **38**(5), 838–846 (1998). https://doi.org/10.1002/pen.10249
13. Kurt, M., Kaynak, Y., Kamber, O.S., Mutlu, B., Bakir, B., Koklu, U.: Influence of molding conditions on the shrinkage and roundness of injection molded parts. Int. J. Adv. Manuf. Technol. **46**(5–8), 571–578 (2010). https://doi.org/10.1007/s00170-009-2149-x
14. Mesogitis, T.S., Skordos, A.A., Long, A.C.: Uncertainty in the manufacturing of fibrous thermosetting composites: a review. Compos. A Appl. Sci. Manuf. **57**(5), 67–75 (2014). https://doi.org/10.1016/j.compositesa.2013.11.004
15. Arsigny, V., Fillard, P., Pennec, X., Ayache, N.: Log-Euclidean metrics for fast and simple calculus on diffusion tensors. Magn. Reson. Med. **56**(2), 411–421 (2006). https://doi.org/10.1002/mrm.20965
16. Ennis, D.B., Kindlmann, G.: Orthogonal tensor invariants and the analysis of diffusion tensor magnetic resonance images. Magn. Reson. Med. **55**(1), 136–146 (2006). https://doi.org/10.1002/mrm.20741
17. Kindlmann, G., Estépar, R.S.J., Niethammer, M., Haker, S., Westin, C.-F.: Geodesic-loxodromes for diffusion tensor interpolation and difference measurement. Medical image computing and computer-assisted intervention : MICCAI … International Conference on Medical Image Computing and Computer-Assisted Intervention **10**(Pt 1), 1–9 (2007). https://doi.org/10.1007/978-3-540-75757-3_1
18. Gahm, J.K., Wisniewski, N., Kindlmann, G., Kung, G.L., Klug, W.S., Garfinkel, A., Ennis, D.B.: Linear invariant tensor interpolation applied to cardiac diffusion tensor MRI. Medical image computing and computer-assisted intervention : MICCAI … International Conference on Medical Image Computing and Computer-Assisted Intervention **15**(Pt 2), 494–501 (2012). https://doi.org/10.1007/978-3-642-33418-4_61
19. Krauß, C., Kärger, L.: Tensor interpolation in virtual manufacturing chains for fiber reinforced composites. Int. J. Mech. Sci. **226**(7), 107378 (2022). https://doi.org/10.1016/j.ijmecsci.2022.107378
20. Blarr, J., Sabiston, T., Krauß, C., Bauer, J.K., Liebig, W.V., Inal, K., Weidenmann, K.A.: Implementation and comparison of algebraic and machine learning based tensor interpolation methods applied to fiber orientation tensor fields obtained from CT images. Comput. Mater. Sci. **228**(3), 112286 (2023). https://doi.org/10.1016/j.commatsci.2023.112286
21. Wittemann, F.: Fiber-dependent injection molding simulation of discontinuous reinforced polymers. Doctoral Thesis, Karlsruhe, Germany (2022)
22. Kamal, M.R., Sourour, S.: Kinetics and thermal characterization of thermoset cure. Polym. Eng. Sci. **13**(1), 59–64 (1973). https://doi.org/10.1002/pen.760130110
23. Wang, J., O'Gara, J.F., Tucker, C.L.: An objective model for slow orientation kinetics in concentrated fiber suspensions: theory and rheological evidence. J. Rheol. **52**(5), 1179–1200 (2008). https://doi.org/10.1122/1.2946437

24. Du Chung, H., Kwon, T.H.: Invariant-based optimal fitting closure approximation for the numerical prediction of flow-induced fiber orientation. J. Rheol. **46**(1), 169–194 (2002). https://doi.org/10.1122/1.1423312
25. Jeffery, G.B.: The motion of ellipsoidal particles immersed in a viscous fluid. Proc. R. Soc. London **102**, 161–179 (1922)
26. Folgar, F., Tucker, C.L.: Orientation Behavior of Fibers in Concentrated Suspensions. J. Reinf. Plast. Compos. **3**, 98–119 (1984)
27. Advani, S.G.: Flow and rheology in polymer composites manufacturing. Composite materials series, vol. 10. Elsevier, Amsterdam, New York (1994)
28. Bay, R.: Fiber Orientation in Injection Molded Composites: A Comparison of Theory and Experiment. Phd. thesis. University of Illinois, Urbana-Campaign (1991)
29. Pipes, R.B., Hearle, J.W.S., Beaussart, A.J., Sastry, A.M., Okine, R.K.: A Constitutive relation for the viscous flow of an oriented fiber assembly. J. Compos. Mater. **25**(9), 1204–1217 (1991). https://doi.org/10.1177/002199839102500907
30. Maertens, R.: Process development and material characterization for the injection molding of long glass fiber-reinforced phenol formaldehyde resins. Doctoral Thesis, Karlsruhe, Germany (2022)
31. Wittemann, F., Kärger, L.: Numerical Study on Uncertainty Effects in Injection Molding. Proceedings 23th International Conference on Composte Materials (ICCM23) (2023). https://doi.org/10.5445/IR/1000165890
32. Höer, M.: Einfluss der Material- und Verarbeitungseigenschaften von Phenolharzformmassen auf die Qualität spritzgegossener Bauteile. Universitätsverlag Chennitz, Chemnitz (2014)
33. Higham, N.J.: Computing a nearest symmetric positive semidefinite matrix. Linear Algebra Appl. **103**, 103–118 (1988). https://doi.org/10.1016/0024-3795(88)90223-6
34. D'Errico J.: nearestSPD, MATLAB Central File Exchange, retrieved Feb. 28, 2023 (2023)